

Reversible Electrochemical Interface of Mg Metal and Conventional Electrolyte Enabled by Intermediate Adsorption

Hui Wang,^{†,§,¶} Xuefei Feng,^{‡,§} Ying Chen,^{○,§} Yi-Sheng Liu,^{‡,§,¶} Kee Sung Han,^{○,§,¶} Mingxia Zhou,^{||,§,¶} Mark H. Engelhard,^{⊥,¶} Vijayakumar Murugesan,^{○,§,¶} Rajeev S. Assary,^{||,§,¶} Tianbiao Leo Liu,[†] Wesley Henderson,[†] Zimin Nie,[†] Meng Gu,[⊥] Jie Xiao,^{†,¶} Chongmin Wang,^{⊥,¶} Kristin Persson,^{◆,§,¶} Donghai Mei,^{○,¶} Ji-Guang Zhang,^{†,¶} Karl T. Mueller,^{○,§,¶} Jinghua Guo,^{‡,§,¶} Kevin Zavadil,^{∇,§,¶} Yuyan Shao,^{*,†,§,¶} and Jun Liu^{†,¶}

[†]Energy & Environment Directorate, Pacific Northwest National Laboratory, Richland, Washington 99352, United States

[‡]Advanced Light Source, Lawrence Berkeley National Laboratory, Berkeley, California 94720, United States

[○]Physical and Computational Sciences Directorate, Pacific Northwest National Laboratory, Richland, Washington 99352, United States

^{||}Materials Science Division, Argonne National Laboratory, 9700 South Cass Avenue, Lemont, Illinois 60439, United States

[⊥]Environmental Molecular Sciences Laboratory, Pacific Northwest National Laboratory, Richland, Washington 99352, United States

[◆]Energy Technologies Area, Lawrence Berkeley National Laboratory, Berkeley, California 94720, United States

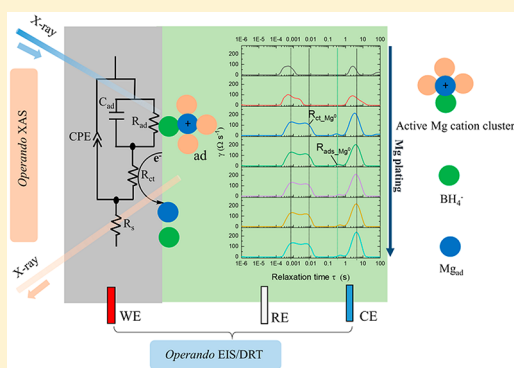
[∇]Material, Physical, and Chemical Sciences, Sandia National Laboratories, Albuquerque, New Mexico 87185, United States

[§]Joint Center for Energy Storage Research (JCESR), Lemont Illinois 60439, United States

[¶]Department of Materials Science and Engineering, University of California, Berkeley, Berkeley, California 94720, United States

Supporting Information

ABSTRACT: Conventional electrolytes made by mixing simple Mg^{2+} salts and aprotic solvents, analogous to those in Li-ion batteries, are incompatible with Mg anodes because Mg metal readily reacts with such electrolytes, producing a passivation layer that blocks Mg^{2+} transport. Here, we report that, through tuning a conventional electrolyte— $Mg(TFSI)_2$ ($TFSI^-$ is $N(SO_2CF_3)_2^-$)—with an $Mg(BH_4)_2$ cosalt, highly reversible Mg plating/stripping with a high Coulombic efficiency is achieved by neutralizing the first solvation shell of Mg cationic clusters between Mg^{2+} and $TFSI^-$ and enhanced reductive stability of free $TFSI^-$. A critical adsorption step between Mg^0 atoms and active Mg cation clusters involving BH_4^- anions is identified to be the key enabler for reversible Mg plating/stripping through analysis of the distribution of relaxation times (DRT) from operando electrochemical impedance spectroscopy (EIS), operando electrochemical X-ray absorption spectroscopy (XAS), nuclear magnetic resonance (NMR), and density functional theory (DFT) calculations.



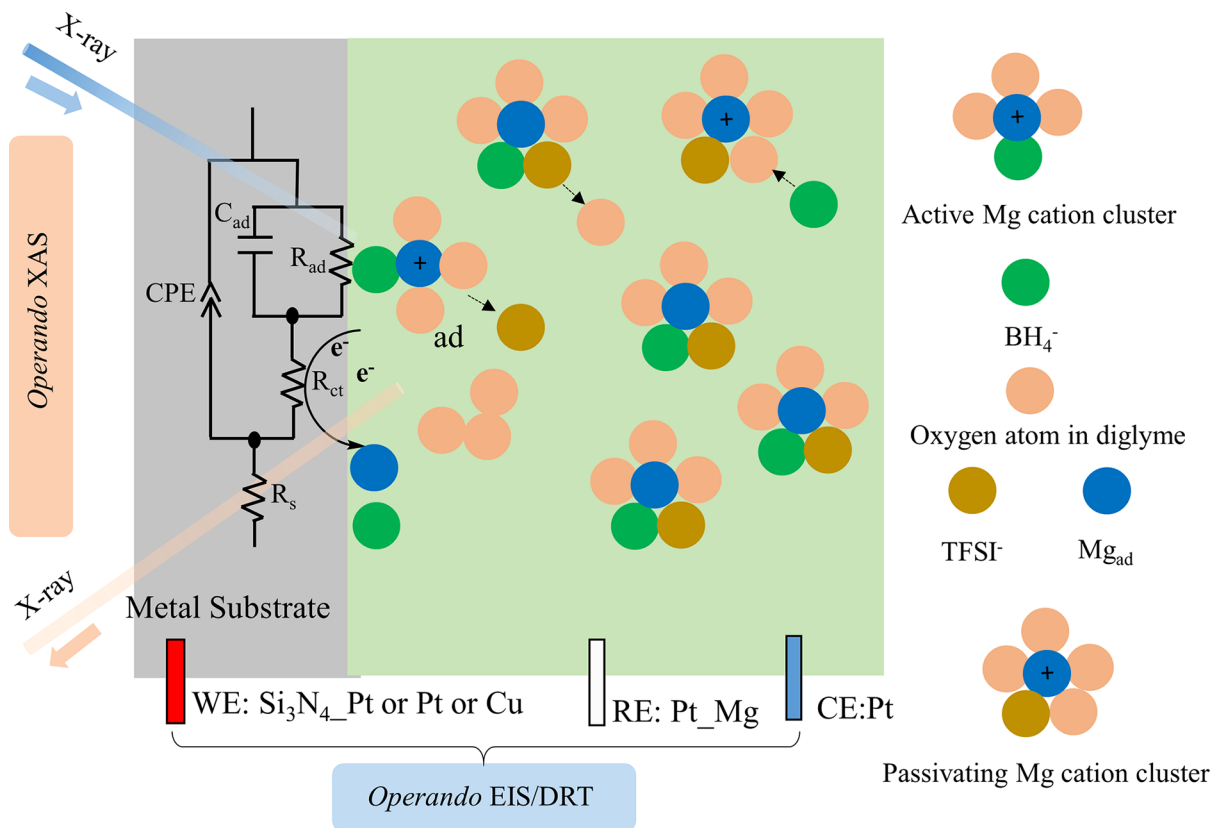
The deployment of large-scale electric energy storage for transportation and electric grid applications stipulates the need for low-cost, safe, and high-energy-density battery technologies.^{1–3} Magnesium batteries are one promising technology that could potentially meet these requirements because of the high volumetric capacity (for comparison: 3832 mAh/cm³_{Mg}, 2062 mAh/cm³_{Li}, and 1136 mAh/cm³_{Na}), better safety (Mg metal anodes can be nondendritic^{4,5} and less chemically reactive than Li or Na metal), and low cost by using the earth-abundant element Mg. Good progress^{6–16} has been

made in the Mg battery field since the first prototype rechargeable Mg battery was reported by Aurbach and co-workers in 2000.¹⁷ Still, significant technical challenges remain, including the limited performance and high incompatibility of electrolytes (with electrode materials) and sluggish solid-state

Received: October 9, 2019

Accepted: December 4, 2019

Published: December 4, 2019

Scheme 1. Schematic Illustration of Probing the Electrified Interface Involving Adsorption of Active Mg Cation Clusters^a

^aMystery roles of Mg cation clusters at electrified interface are unveiled by a coupled method of operando soft XAS and EIS and corresponding DRT analysis. Typical conventional Mg electrolytes (i.e. $\text{Mg}(\text{N}(\text{CF}_3\text{SO}_2)_2)$ in diglyme), with/without cosalt of $\text{Mg}(\text{BH}_4)_2$, are studied to correlate the solvate composition with potential-dependent Mg plating/stripping reactivity.

transfer kinetics of Mg^{2+} cations. In addition, limited fundamental understanding of Mg electrolyte/electrode interfaces presents a scientific challenge for design and development of better materials for Mg batteries.^{18,19}

Elucidating the electrolyte-dependent reversible Mg plating/stripping at the electrified interface is thus of pivotal importance to design and develop electrolytes.^{20,21} Adsorption of active intermediate Mg^+ clusters ($[\text{MgX}]^+$) has been identified to be a vital step for reversible Mg plating/stripping by operando electrochemical X-ray absorption spectroscopy (XAS).^{22,23} However, it is still hard to detect the $[\text{M}\cdots\text{Mg}]_{\text{ad}}$ state (i.e., a transient charge-transfer reaction intermediate) by operando XAS during the charge-transfer reaction, i.e., $\text{M} + [\text{MgX}]_{\text{ad}}^+ + 2\text{e}^- \rightarrow [\text{M}\cdots\text{Mg}]_{\text{ad}} + \text{X}^-$ (a key step of Mg plating) due to the fast diffusion rate of Mg adatoms on the substrate surface.²² Operando electrochemical impedance spectroscopy (EIS) has gained wide popularity as a nondestructive, sensitive, and highly informative method to explore the interfaces between metal electrodes and liquid electrolytes, which is complementary to operando XAS, particularly for charge-transfer reactions involving the adsorption step of active redox species.²⁴ However, it is still challenging to distinguish electrochemical processes with comparable time constants from the complex impedance spectrum. Recently, a new method of distribution of relaxation times (DRT), based on analysis of the measured impedance spectrum, has been established to interpret the complex electrochemical process with a much higher resolution.^{25,26} Especially, DRT analysis is an effective method in unveiling the emergence of new

electrochemical processes (e.g., new surface film at electrodes, new charge transfer, new adsorption, etc.) at evolving electrified interfaces.^{27,28} An integrated operando method (Scheme 1) is then proposed to probe the electrified Mg/electrolyte interface.

In this Letter, we used $\text{Mg}(\text{BH}_4)_2$ as cosalt, together with a conventional electrolyte composition, i.e., $\text{Mg}(\text{TFSI})_2$ (TFSI^- is the bis(trifluoromethanesulfonyl)imide anion $\text{N}(\text{SO}_2\text{CF}_3)_2^-$) in diglyme, to study the Mg/electrolyte interface with the aim to identify key reaction steps for reversible Mg electrochemistry. A highly reversible Mg plating/stripping is achieved by neutralizing the first solvation shell of Mg cationic clusters between Mg^{2+} and TFSI^- and enhanced reductive stability of free TFSI^- . The charge-transfer reaction with adsorption of active Mg cation clusters involving BH_4^- is identified by a set of operando analysis tools to be the key mechanism for reversible Mg plating/stripping.

Magnesium electrochemistry is first studied in the conventional electrolyte 0.2 M $\text{Mg}(\text{TFSI})_2$ in diglyme. Figure 1a shows the cyclic voltammogram (CV) with a Pt working electrode in 0.2 M $\text{Mg}(\text{TFSI})_2/\text{diglyme}$. A reduction peak occurs below -0.4 V, with a small oxidation peak near 0.4 V and a larger oxidation peak near 2.0 V (vs Mg). An electrochemical experiment was designed to identify these peaks. Mg metal was initially electrodeposited from a Mg electrolyte (it has been confirmed that only Mg^0 was deposited).²⁹ The Mg^0 was then rinsed with diglyme and transferred to a cell with the 0.2 M $\text{Mg}(\text{TFSI})_2/\text{diglyme}$ electrolyte. The electrochemical stripping of the Mg^0 was

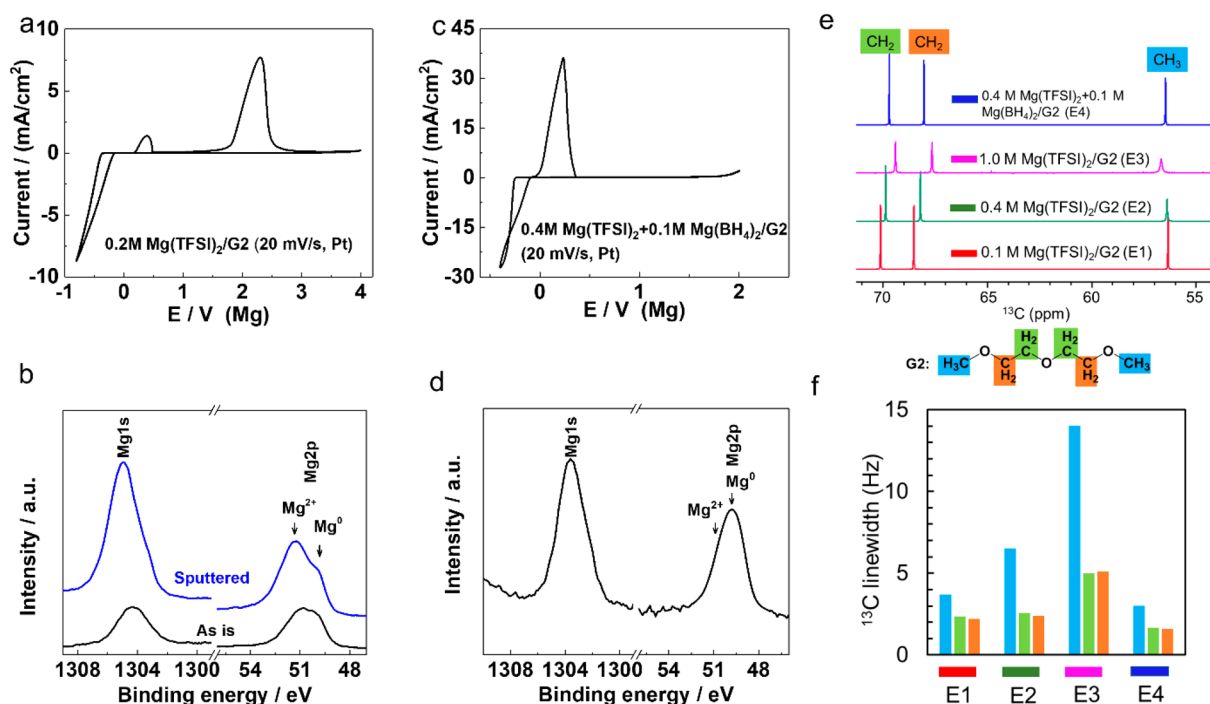


Figure 1. BH_4^- -dictated reversible Mg electrochemistry. (a) CV (20 mV/s on Pt) in 0.2 M $\text{Mg}(\text{TFSI})_2/\text{diglyme}$; (b) XPS patterns of the Mg deposition from 0.2 M $\text{Mg}(\text{TFSI})_2/\text{diglyme}$; (c) CV (20 mV/s on Pt) in 0.4 M $\text{Mg}(\text{TFSI})_2 + 0.1 \text{ M Mg}(\text{BH}_4)_2/\text{diglyme}$; (d) XPS patterns of the Mg deposition from 0.4 M $\text{Mg}(\text{TFSI})_2 + 0.1 \text{ M Mg}(\text{BH}_4)_2/\text{diglyme}$; (e) ^{13}C NMR spectra; and (f) line width of three carbon resonances of diglyme with $\text{Mg}(\text{TFSI})_2$ concentration varying from 0.1 to 1 M without and with 0.1 M $\text{Mg}(\text{BH}_4)_2$ cosalt. E1: 0.1 M $\text{Mg}(\text{TFSI})_2$ in G2; E2: 0.4 M $\text{Mg}(\text{TFSI})_2$ in G2; E3: 1.0 M $\text{Mg}(\text{TFSI})_2$ in G2; E4: 0.4 M $\text{Mg}(\text{TFSI})_2 - 0.1 \text{ M Mg}(\text{BH}_4)_2$ in G2.

carried out after holding the electrode in the electrolyte for a certain period of time (0, 1, and 5 min, respectively). With increasing holding time, a dramatic decrease in the peak at 0.4 V is observed in Figure S1a. This decrease is clearly linked with the corresponding increase in the second peak at 2.0 V. It can be deduced from the peak evolution, peak potential, and Mg electrochemistry in “Mg electrolytes” (i.e., other electrolyte formulations that do enable highly reversible Mg plating/stripping) that the first oxidation peak (0.4 V) is ascribed to the electrochemical dissolution of Mg^0 and the second peak (2.0 V) to the oxidation of reaction products formed from the side reaction between Mg^0 and the electrolyte components (specifically the TFSI^- anion; see the SI); the reduction peak below -0.4 V (Figure 1a) is due to the electrochemical deposition of Mg metal. It is thus clear that Mg^0 can be electrodeposited from the conventional electrolyte without a cosalt (see further information in the following physicochemical characterization). Once Mg^0 is formed, however, it rapidly reacts with the conventional electrolyte, resulting in Mg reaction products that can only be oxidized at high overvoltage. The reaction(s) take(s) place on a time scale of minutes with an estimated $t_{1/2}$ of less than 30 s (Figure S1a). By controlling the reaction time, the Mg^0 that has not reacted with the electrolyte can be electrochemically stripped at low potential (i.e., the peak noted at 0.4 V).

In contrast to these results, when small amounts of $\text{Mg}(\text{BH}_4)_2$ salt are added to the 0.2 M $\text{Mg}(\text{TFSI})_2/\text{diglyme}$ electrolyte, dramatic changes of the electrochemical stripping of Mg^0 occur (Figure S1b). Only the oxidation peak at low overpotential (0.4 V) is observed, and this peak does not change with holding time in the electrolyte. This inspired us to further explore this system to understand the fundamental mechanisms that is responsible for the change in behavior from

the pure $\text{Mg}(\text{TFSI})_2$ system and the implications for reversible Mg electrochemistry.

Upon the basis of the above observations, we used $\text{Mg}(\text{BH}_4)_2$ as an cosalt to prepare a 0.4 M $\text{Mg}(\text{TFSI})_2 - 0.1 \text{ M Mg}(\text{BH}_4)_2/\text{diglyme}$ electrolyte, in which we observed highly reversible Mg plating/stripping, and the Coulombic efficiency (CE) was calculated to be 98.8%. The XRD pattern (Figure S4) shows that Mg metal was deposited, and the SEM image of the surface (Figure S4) shows a smooth and dendrite-free Mg deposition morphology. The XPS analysis exhibits Mg peaks for the Mg deposition (Figure 1d) and no Mg signal after stripping, indicating fully reversible Mg plating/stripping processes. No F, S, N, or B signals are observed on Mg deposition (Figure S5). The narrow peak for the high-resolution XPS Mg 2p peak (Figure 1d) indicates a simple Mg composition, most of which is Mg^0 with little or no Mg^{2+} ,³⁰ in drastic contrast to the observations in Figure 1b. This confirms that with the $\text{Mg}(\text{BH}_4)_2$ cosalt Mg^0 does not react with or decompose the TFSI^- anions present in the electrolyte.

To investigate the change of the chemical environment of bulk electrolytes by $\text{Mg}(\text{BH}_4)_2$ cosalt, solution-state ^1H , ^{13}C , ^{19}F , and ^{11}B NMR measurements were carried out to provide molecular-level structural and dynamic information on diglyme, TFSI^- , and BH_4^- . As shown in Figure 1e,f, by increasing $\text{Mg}(\text{TFSI})_2$ concentration from 0.1 to 1 M, the ^{13}C line widths of the three carbon species in diglyme increase, indicating that the mobility of diglyme is significantly reduced due to its coordination to Mg^{2+} in solution. When 0.1 M $\text{Mg}(\text{BH}_4)_2$ is introduced to 0.4 M $\text{Mg}(\text{TFSI})_2/\text{diglyme}$, the ^{13}C line widths of all three carbon resonances drop dramatically, suggesting an enhancement in the diglyme mobility. ^1H NMR shows the same trend (Figure S6), a rapid decrease in ^1H spin–spin relaxation time (T_2) by increasing $\text{Mg}(\text{TFSI})_2$

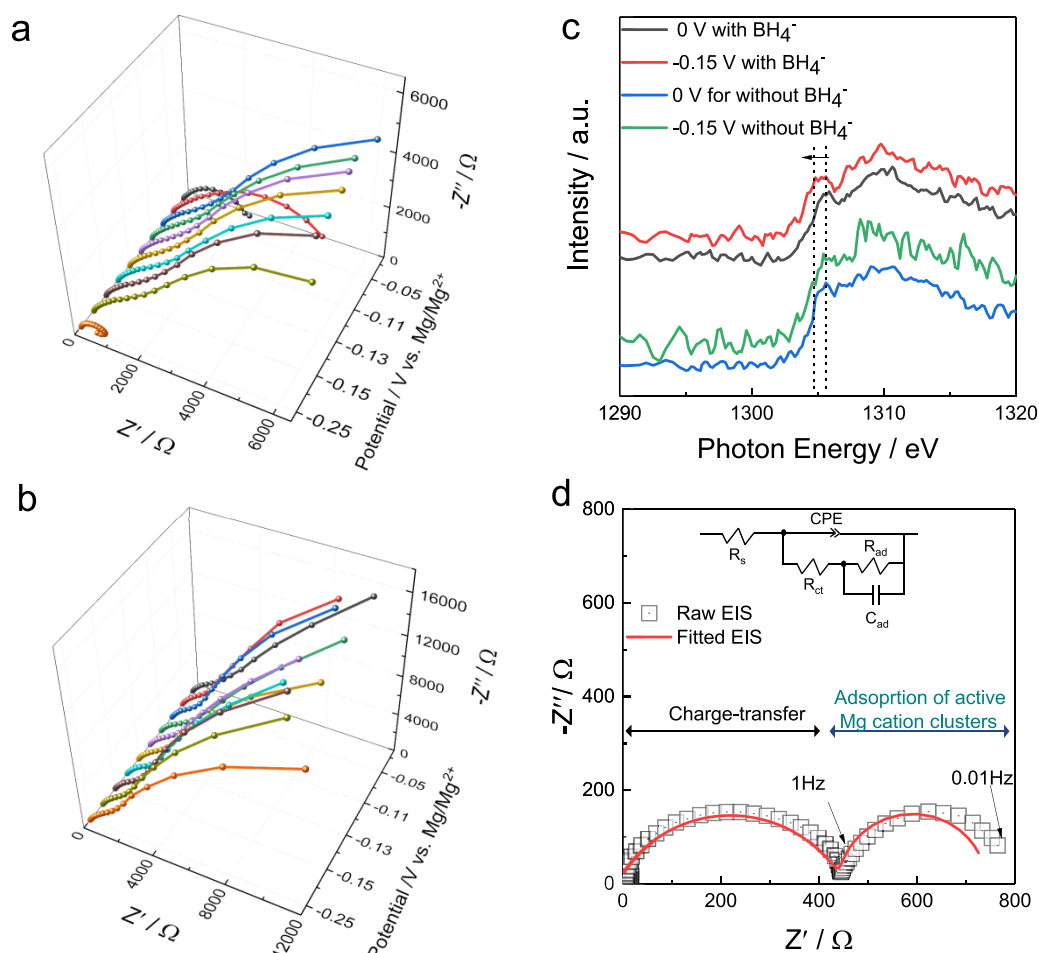


Figure 2. Evidence of the adsorption of active Mg cation clusters with BH_4^- . Potential-dependent impedance evolution of the working electrode of the Pt disk in a three-electrode Swagelok cell (Pt: WE; Mg: RE; Mg: CE) using 0.4 M $\text{Mg}(\text{TFSI})_2 + 0.1$ M $\text{Mg}(\text{BH}_4)_2/\text{diglyme}$ (a) and 0.4 M $\text{Mg}(\text{TFSI})_2/\text{diglyme}$ (b); (c) pre-edge evolution of the X-ray absorption near-edge spectroscopy (XANES) region of the Mg K-edge upon cathodic sweeping from 0 to -0.15 V (i.e., prior to the onset Mg electrodeposition) between the interface of Pt and 0.4 M $\text{Mg}(\text{TFSI})_2 + 0.1$ M $\text{Mg}(\text{BH}_4)_2/\text{diglyme}$ or 0.4 M $\text{Mg}(\text{TFSI})_2/\text{diglyme}$; (d) typical impedance spectrum and corresponding fitted one with a loop in the lower frequency range using electrolyte with $\text{Mg}(\text{BH}_4)_2$ after Mg bulk electrodeposition. The proposed electrical equivalent circuit is a typical one of modeling the faradic reactions in the presence of one adsorption species.

concentration and a remarkable increase with the addition of 0.1 M $\text{Mg}(\text{BH}_4)_2$, confirming the faster solvent motion enabled by $\text{Mg}(\text{BH}_4)_2$ cosalt. ^{19}F NMR spectra of 0.4 M $\text{Mg}(\text{TFSI})_2/\text{diglyme}$ and $\text{Mg}(\text{TFSI})_2-\text{Mg}(\text{BH}_4)_2/\text{diglyme}$ exhibit little change in chemical shift but a slight line broadening (reduced T_2) in the mixture, while ^{11}B NMR spectra of $\text{Mg}(\text{BH}_4)_2/\text{diglyme}$ and $\text{Mg}(\text{TFSI})_2-\text{Mg}(\text{BH}_4)_2/\text{diglyme}$ display identical pentet B resonances centered at -42.23 and -42.28 ppm, respectively, and also a slight line broadening in the mixture. Combining these observations with a previous Mg NMR and computational modeling study on the same system,³¹ we have thus harvested a complete picture of the change in solvation structures and molecular dynamics by addition of $\text{Mg}(\text{BH}_4)_2$. Because TFSI^- is a weakly coordinating anion, $\text{Mg}(\text{TFSI})_2$ is expected to mostly dissociate at low concentrations (0.1 M) and form contact the ion pair at a higher concentration (0.4 M) with the dominant solvation structure $[\text{Mg}(\text{TFSI})^+(\text{diglyme})_2]$ (Scheme S1).⁶ Because two diglyme molecules are involved in the first solvation shell, solvent mobility decreases with Mg^{2+} concentration, especially for the

terminal CH_3 , due to the coordination between neighboring oxygen and Mg^{2+} . In contrast, BH_4^- is a much stronger coordinating ligand and forms stable ion association $[\text{Mg}(\text{BH}_4)_2(\text{diglyme})]$ even at a very low concentration (0.01 M). In the mixture of 0.4 M $\text{Mg}(\text{TFSI})_2$ and 0.1 M $\text{Mg}(\text{BH}_4)_2$, both TFSI^- and BH_4^- anions maintain in the first solvation shell, as suggested by the unaltered ^{19}F and ^{11}B NMR. The significantly elevated solvent dynamics demonstrated by ^1H and ^{13}C NMR compared to the neat $\text{Mg}(\text{TFSI})_2$ solution indicates the release of diglyme from the first solvation shell. This is consistent with the solvation structure $[\text{Mg}(\text{BH}_4)(\text{TFSI})(\text{diglyme})]$ obtained from ^{25}Mg NMR studies.³¹ The chemical environment of Mg^{2+} is significantly changed by addition of BH_4^- ; the first solvation shell of contact ion pairs between Mg^{2+} and TFSI^- is accordingly neutralized (Scheme 1), which significantly inhibits the reduction of TFSI^- in the monocationic Mg clusters (i.e., $[\text{Mg}(\text{TFSI})^+(\text{DGM})_2]$) accessible to the substrate during Mg plating.³² However, the role of active Mg^+ clusters with BH_4^- in reversible Mg electrochemistry on an electrified interface is still unknown.

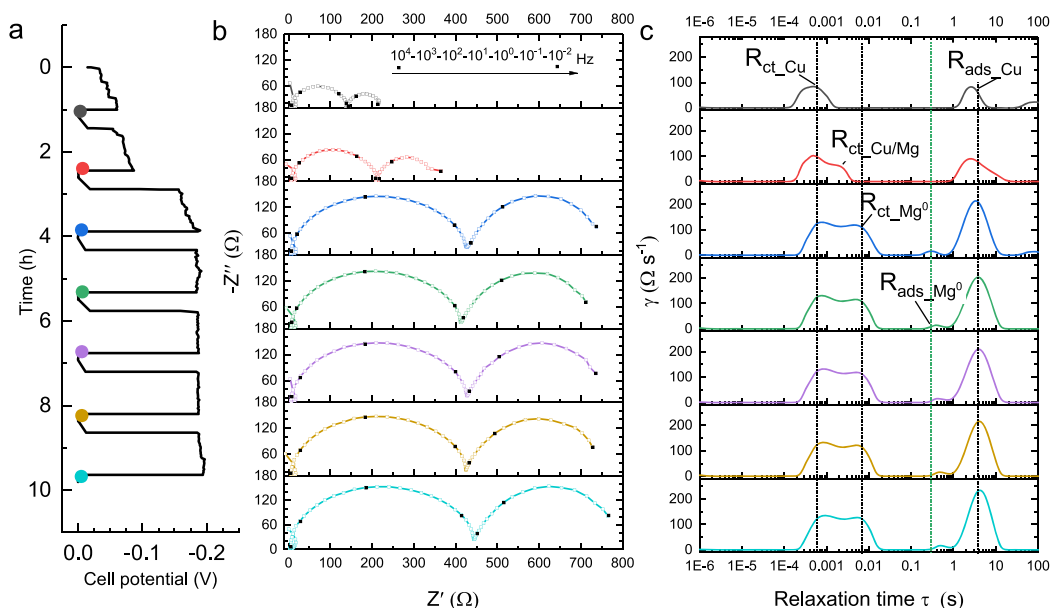


Figure 3. Adsorption-dependent nonpassivation. Operando EIS evolution and corresponding analysis of DRT upon galvanostatic electrodeposition of Mg onto Cu at 0.5 mA cm^{-2} in $0.4 \text{ M Mg(TFSI)}_2 + 0.1 \text{ M Mg(BH}_4)_2/\text{diglyme}$. (a) Discharge cell potential vs time curve; (b) evolution of recorded impedance spectra in the frequency range of 10^6 – 0.01 Hz ; (c) corresponding DRT spectra.

Figure 2a,b shows potential-dependent operando EIS evolution of the working electrode of a Pt disk in a three-electrode Swagelok cell (Figure S7) using electrolytes with/without BH_4^- . As we pointed out at the beginning, the adsorption step of key intermediates is critical for reversible Mg plating/stripping; here we try to identify the adsorption intermediates if any. Operando EIS has been developed to identify the adsorption intermediates.^{24,33} For the cell using electrolyte with BH_4^- , the impedance of the Pt working electrode substantially increases upon sweeping from 0 to -0.10 V , then gradually decreases from -0.10 to -0.20 V , and then suddenly decreases at -0.25 V due to the Mg electrodeposition. The initial impedance increase is probably associated with the generation of a negative-charged Pt surface to repel anions. The later gradual decrease likely originates from the continuous adsorption of active cationic clusters (e.g., $(\text{MgBH}_4)^+$; this step involves the repelling of TFSI^- in neutralized solvation shells away from the Pt working electrode). However, a totally different scenario was observed for the cell using electrolytes without BH_4^- . No significant impedance change was observed in the full cathodic sweep from 0 to -0.20 V , indicating no occurrence of effective adsorption and bulk electrodeposition. To further confirm the adsorption step prior to the onset of Mg electrodeposition, operando potentiostatic XAS was performed at 0 and -0.15 V for both electrolytes using the three-electrode homemade cell (Figure S7). Figure 2c shows an obvious shift to the low-energy edge (i.e., to the energy of Mg metal) for the cell using electrolyte with BH_4^- but not for the cell using electrolyte without BH_4^- .²¹ The pre-edge shift of the Mg K-edge can be useful to probe the near-surface region of the electrolyte if there is a chemical difference for the new species with respect to the bulk components. The observed shift should be largely associated with active Mg cation clusters involving BH_4^- adsorbed at the Pt/electrolyte interface before the onset of Mg electrodeposition. A similar shift was observed in other electrolytes that contain Mg adsorption intermediates to enable reversible Mg plating/stripping.^{21,22} Despite low

signal-to-noise ratios stemming from a low beam flux at the Mg K-edge energy, the spectra were collected in one experiment, and the energy shift was clearly identified. Further, the adsorption of active Mg cation clusters involving BH_4^- was demonstrated, after Mg bulk electrodeposition, by the presence of a loop for the Cu working electrode (Figure S7) in the lower-frequency range of 1 – 0.01 Hz in Figure 2d.²⁴ The proposed electrical equivalent circuit is often used to model the faradic reactions with one adsorption species, and the fitted spectrum is close to that of the raw one, indicating the rationality and validity of this electrical equivalent circuit.²⁴ Besides, preliminary periodic density functional theory (DFT) calculations (Figure S8) indicate a thermodynamically favorable coordination interaction between BH_4^- and the Mg surface as compared to TFSI^- .

Operando EIS evolution of galvanostatic electrodeposited Mg onto Cu was recorded during the OCV resting period at 0.5 mA cm^{-2} every hour in $0.4 \text{ M Mg(TFSI)}_2 + 0.1 \text{ M Mg(BH}_4)_2/\text{diglyme}$ in Figure 3. The loop was always observed in the low-frequency range (1 – 0.01 Hz) during the steady galvanostatic Mg electrodeposition, indicating the sustainable presence of an adsorption (R_{ads}) by intermediate active Mg cation clusters.²⁴ The first loop in the high-frequency range is associated with the charge-transfer process (R_{ct}), which evolved into a steady state when the cell potential reached ca. -0.18 V . Post-mortem analysis of corresponding DRT spectra show peaks for R_{ct} in the high-frequency range (i.e., 10^4 – 10^2 Hz) and for R_{ads} in the middle–low-frequency range (i.e., 10 – 0.01 Hz), which align well with the proposed electrical equivalent circuit in Figure 2d. DRT results also clearly present the evolving interface in detail, without the fitting process, in terms of the evolution of the charge-transfer process (i.e., from $R_{\text{ct,Cu}}$ to $R_{\text{ct,Mg}^0}$) and the emergence of a new adsorption step ($R_{\text{ads,Mg}^0}$). Both new peaks are associated with newly formed Mg electrodeposits onto the Cu substrate. Especially, the charge-transfer reaction with the adsorption step of active Mg clusters onto Mg electrodeposits is uncovered by the DRT analysis.

However, Figure S9 shows a totally different scenario for the cell without addition of $\text{Mg}(\text{BH}_4)_2$. Galvanostatic electro-deposition of Mg onto Cu is terminated by the passivation with the emergence of the second large semicircle in the middle–low-frequency range (10–0.1 Hz) and an inclined line ($R_{\text{warburg_Mg}}^0$; 0.1–0.01 Hz), which can be explained by the modified Randle circuit. DRT analysis suggests that the charge-transfer process ($R_{\text{ct_Mg}}^0$) is a dominant electrochemical process at ca. 10 Hz, and the migration of Mg^{2+} toward this surface film (i.e. $R_{\text{SEI_Mg}}^0$) is sluggish, which is revealed by the peak positioned at a middle frequency of ca. 400 Hz, analogous to the reported typical frequency range for SEI (1 kHz to 10 Hz) and for the charge-transfer process (10 Hz to mHz) in Li-ion batteries.²⁵ It is thus concluded that nonpassivation is driven by the adsorption of active Mg cation clusters with BH_4^- .

In summary, the stronger interaction between Mg^0 , Mg^{2+} , and BH_4^- (as compared to TFSI^-) is revealed to render a preferred absorption (but not decomposition) of the BH_4^- anions on the Mg metal surface during the charge-transfer reaction. This in turn prevents undesirable side reactions between the Mg^0 and passivating Mg cationic clusters with TFSI^- , thus allowing highly reversible Mg plating/stripping. The adsorption mechanism may plausibly be extended to other multivalent electrolyte systems.

■ ASSOCIATED CONTENT

Supporting Information

The Supporting Information is available free of charge at <https://pubs.acs.org/doi/10.1021/acseenergylett.9b02211>.

Experimental and characterization section and additional experimental results, including EIS, XAS, NMR, XPS, XRD, and DFT calculations (PDF)

■ AUTHOR INFORMATION

Corresponding Author

*E-mail: yuyan.shao@pnnl.gov.

ORCID

Hui Wang: 0000-0003-1997-2312

Yi-Sheng Liu: 0000-0002-1085-1947

Kee Sung Han: 0000-0002-3535-1818

Mingxia Zhou: 0000-0002-1896-1024

Mark H. Engelhard: 0000-0002-5543-0812

Vijayakumar Murugesan: 0000-0001-6149-1702

Rajeev S. Assary: 0000-0002-9571-3307

Jie Xiao: 0000-0002-5520-5439

Chongmin Wang: 0000-0003-3327-0958

Donghai Mei: 0000-0002-0286-4182

Ji-Guang Zhang: 0000-0001-7343-4609

Karl T. Mueller: 0000-0001-9609-9516

Jinghua Guo: 0000-0002-8576-2172

Kevin Zavadil: 0000-0002-3791-424X

Yuyan Shao: 0000-0001-5735-2670

Jun Liu: 0000-0001-8663-7771

Present Address

[†]College of Chemistry and Chemical Engineering, Tianjin Polytechnic University, Tianjin 300387, P. R. China.

Notes

The authors declare no competing financial interest.

■ ACKNOWLEDGMENTS

This work was supported as part of the Joint Center for Energy Storage Research (JCESR), an Energy Innovation Hub funded by the U.S. Department of Energy (DOE), Office of Science, Basic Energy Sciences. The XPS/SEM were performed at the Environmental Molecular Sciences Laboratory (EMSL), a national scientific user facility sponsored by the DOE Office of Biological and Environmental Research and located at Pacific Northwest National Laboratory (PNNL). The operando XAS work at the Advanced Light Source of Lawrence Berkeley National Laboratory (LBNL) was supported by the Director of the Office of Science, Office of Basic Energy Sciences, of DOE under Contract No. DEAC02-05CH11231. We gratefully acknowledge the computing resources provided on “BEBOP”, a computing cluster operated by the Laboratory Computing Resource Center at Argonne National Laboratory (ANL).

■ REFERENCES

- (1) Dunn, B.; Kamath, H.; Tarascon, J.-M. Electrical Energy Storage for the Grid: A Battery of Choices. *Science* **2011**, *334* (6058), 928–935.
- (2) Yang, Z.; Zhang, J.; Kintner-Meyer, M. C. W.; Lu, X.; Choi, D.; Lemmon, J. P.; Liu, J. Electrochemical Energy Storage for Green Grid. *Chem. Rev.* **2011**, *111* (5), 3577–3613.
- (3) Liu, J.; Zhang, J.-G.; Yang, Z.; Lemmon, J. P.; Imhoff, C.; Graff, G. L.; Li, L.; Hu, J.; Wang, C.; Xiao, J.; Xia, G.; Viswanathan, V. V.; Baskaran, S.; Sprenkle, V.; Li, X.; Shao, Y.; Schwenzler, B. Materials Science and Materials Chemistry for Large Scale Electrochemical Energy Storage: From Transportation to Electrical Grid. *Adv. Funct. Mater.* **2013**, *23* (8), 929–946.
- (4) Matsui, M. Study on electrochemically deposited Mg metal. *J. Power Sources* **2011**, *196* (16), 7048–7055.
- (5) Ling, C.; Banerjee, D.; Matsui, M. Study of the electrochemical deposition of Mg in the atomic level: Why it prefers the non-dendritic morphology. *Electrochim. Acta* **2012**, *76*, 270–274.
- (6) Rajput, N. N.; Seguin, T. J.; Wood, B. M.; Qu, X.; Persson, K. A. Elucidating Solvation Structures for Rational Design of Multivalent Electrolytes—A Review. *Top. Curr. Chem.* **2018**, *376* (3), 19.
- (7) Muldoon, J.; Bucur, C. B.; Gregory, T. Quest for Nonaqueous Multivalent Secondary Batteries: Magnesium and Beyond. *Chem. Rev.* **2014**, *114* (23), 11683–11720.
- (8) Canepa, P.; Sai Gautam, G.; Hannah, D. C.; Malik, R.; Liu, M.; Gallagher, K. G.; Persson, K. A.; Ceder, G. Odyssey of Multivalent Cathode Materials: Open Questions and Future Challenges. *Chem. Rev.* **2017**, *117* (5), 4287–4341.
- (9) Mao, M.; Gao, T.; Hou, S.; Wang, C. A critical review of cathodes for rechargeable Mg batteries. *Chem. Soc. Rev.* **2018**, *47* (23), 8804–8841.
- (10) Hahn, N. T.; Seguin, T. J.; Lau, K.-C.; Liao, C.; Ingram, B. J.; Persson, K. A.; Zavadil, K. R. Enhanced Stability of the Carba-closedodecaborate Anion for High-Voltage Battery Electrolytes through Rational Design. *J. Am. Chem. Soc.* **2018**, *140* (35), 11076–11084.
- (11) Luo, J.; Bi, Y.; Zhang, L.; Zhang, X.; Liu, T. L. A Stable, Non-corrosive Perfluorinated Pinacolatoborate Mg Electrolyte for Rechargeable Mg Batteries. *Angew. Chem., Int. Ed.* **2019**, *58* (21), 6967–6971.
- (12) Du, A.; Zhang, Z.; Qu, H.; Cui, Z.; Qiao, L.; Wang, L.; Chai, J.; Lu, T.; Dong, S.; Dong, T.; Xu, H.; Zhou, X.; Cui, G. An efficient organic magnesium borate-based electrolyte with non-nucleophilic characteristics for magnesium–sulfur battery. *Energy Environ. Sci.* **2017**, *10* (12), 2616–2625.
- (13) Yoo, H. D.; Liang, Y.; Dong, H.; Lin, J.; Wang, H.; Liu, Y.; Ma, L.; Wu, T.; Li, Y.; Ru, Q.; Jing, Y.; An, Q.; Zhou, W.; Guo, J.; Lu, J.; Pantelides, S. T.; Qian, X.; Yao, Y. Fast kinetics of magnesium monochloride cations in interlayer-expanded titanium disulfide for magnesium rechargeable batteries. *Nat. Commun.* **2017**, *8* (1), 339.

(14) Mizrahi, O.; Amir, N.; Pollak, E.; Chusid, O.; Marks, V.; Gottlieb, H.; Larush, L.; Zinigrad, E.; Aurbach, D. Electrolyte Solutions with a Wide Electrochemical Window for Rechargeable Magnesium Batteries. *J. Electrochem. Soc.* **2008**, *155* (2), A103–A109.

(15) Guo, Y.-s.; Zhang, F.; Yang, J.; Wang, F.-f.; NuLi, Y.; Hirano, S.-i. Boron-based electrolyte solutions with wide electrochemical windows for rechargeable magnesium batteries. *Energy Environ. Sci.* **2012**, *5* (10), 9100–9106.

(16) Gao, X.; Mariani, A.; Jeong, S.; Liu, X.; Dou, X.; Ding, M.; Moretti, A.; Passerini, S. Prototype rechargeable magnesium batteries using ionic liquid electrolytes. *J. Power Sources* **2019**, *423*, 52–59.

(17) Aurbach, D.; Lu, Z.; Schechter, A.; Gofer, Y.; Gizbar, H.; Turgeman, R.; Cohen, Y.; Moshkovich, M.; Levi, E. Prototype systems for rechargeable magnesium batteries. *Nature* **2000**, *407*, 724.

(18) Aurbach, D.; Schechter, A.; Moshkovich, M.; Cohen, Y. On the Mechanisms of Reversible Magnesium Deposition Processes. *J. Electrochem. Soc.* **2001**, *148* (9), A1004–A1014.

(19) Gershinsky, G.; Yoo, H. D.; Gofer, Y.; Aurbach, D. Electrochemical and Spectroscopic Analysis of Mg²⁺ Intercalation into Thin Film Electrodes of Layered Oxides: V₂O₅ and MoO₃. *Langmuir* **2013**, *29* (34), 10964–10972.

(20) Ta, K.; See, K. A.; Gewirth, A. A. Elucidating Zn and Mg Electrodeposition Mechanisms in Nonaqueous Electrolytes for Next-Generation Metal Batteries. *J. Phys. Chem. C* **2018**, *122* (25), 13790–13796.

(21) Arthur, T. S.; Glans, P.-A.; Matsui, M.; Zhang, R.; Ma, B.; Guo, J. Mg deposition observed by in situ electrochemical Mg K-edge X-ray absorption spectroscopy. *Electrochem. Commun.* **2012**, *24*, 43–46.

(22) Benmayza, A.; Ramanathan, M.; Arthur, T. S.; Matsui, M.; Mizuno, F.; Guo, J.; Glans, P.-A.; Prakash, J. Effect of Electrolytic Properties of a Magnesium Organohaloaluminate Electrolyte on Magnesium Deposition. *J. Phys. Chem. C* **2013**, *117* (51), 26881–26888.

(23) Ye, Y.; Wu, C. H.; Zhang, L.; Liu, Y.-S.; Glans-Suzuki, P.-A.; Guo, J. Using soft x-ray absorption spectroscopy to characterize electrode/electrolyte interfaces in-situ and operando. *J. Electron Spectrosc. Relat. Phenom.* **2017**, *221*, 2–9.

(24) Lasia, A., Impedance of the Faradaic Reactions in the Presence of Adsorption. In *Electrochemical Impedance Spectroscopy and its Applications*; Springer: New York, Heidelberg, Dordrecht, London, 2014; pp 131–145.

(25) Steinhauer, M.; Risse, S.; Wagner, N.; Friedrich, K. A. Investigation of the Solid Electrolyte Interphase Formation at Graphite Anodes in Lithium-Ion Batteries with Electrochemical Impedance Spectroscopy. *Electrochim. Acta* **2017**, *228*, 652–658.

(26) Heinzmann, M.; Weber, A.; Ivers-Tiffée, E. Advanced impedance study of polymer electrolyte membrane single cells by means of distribution of relaxation times. *J. Power Sources* **2018**, *402*, 24–33.

(27) Ivers-Tiffée, E.; Weber, A. Evaluation of electrochemical impedance spectra by the distribution of relaxation times. *J. Ceram. Soc. Jpn.* **2017**, *125* (4), 193–201.

(28) Weiß, A.; Schindler, S.; Galbiati, S.; Danzer, M. A.; Zeis, R. Distribution of Relaxation Times Analysis of High-Temperature PEM Fuel Cell Impedance Spectra. *Electrochim. Acta* **2017**, *230*, 391–398.

(29) Shao, Y.; Liu, T.; Li, G.; Gu, M.; Nie, Z.; Engelhard, M.; Xiao, J.; Lv, D.; Wang, C.; Zhang, J.-G.; Liu, J. Coordination Chemistry in magnesium battery electrolytes: how ligands affect their performance. *Sci. Rep.* **2013**, *3*, 3130.

(30) Ardizzone, S.; Bianchi, C. L.; Fadoni, M.; Vercelli, B. Magnesium salts and oxide: an XPS overview. *Appl. Surf. Sci.* **1997**, *119* (3), 253–259.

(31) Hu, J. Z.; Rajput, N. N.; Wan, C.; Shao, Y.; Deng, X.; Jaegers, N. R.; Hu, M.; Chen, Y.; Shin, Y.; Monk, J.; Chen, Z.; Qin, Z.; Mueller, K. T.; Liu, J.; Persson, K. A. 25Mg NMR and computational modeling studies of the solvation structures and molecular dynamics in magnesium based liquid electrolytes. *Nano Energy* **2018**, *46*, 436–446.

(32) Rajput, N. N.; Qu, X.; Sa, N.; Burrell, A. K.; Persson, K. A. The Coupling between Stability and Ion Pair Formation in Magnesium Electrolytes from First-Principles Quantum Mechanics and Classical Molecular Dynamics. *J. Am. Chem. Soc.* **2015**, *137* (9), 3411–3420.

(33) Liu, Y.; Wang, W. Investigation on the Cu(II) and Co(II) Electrochemical Reduction Process in Citrate Solution by CV and EIS. *J. Electrochem. Soc.* **2012**, *159* (6), D375–D381.

NOTE ADDED AFTER ASAP PUBLICATION

This paper was published ASAP on December 13, 2019, with an error in Scheme 1. The corrected version was reposted on December 16, 2019.